Infrared and near Infrared Spectroscopy of Acetylacetone And Hexafluoroacetylacetone

Journal:	*The Journal of Physical Chemistry*
Manuscript ID:	jp-2015-01863x.R1
Manuscript Type:	Article
Date Submitted by the Author:	17-Apr-2015
Complete List of Authors:	Howard, Daryl; Australian Synchrotron, Kjaergaard, Henrik; Copenhagen University, Chemistry Huang, Jing; University of Basel, Meuwly, Markus; University, Chemistry

Infrared and Near Infrared Spectroscopy of Acetylacetone and Hexafluoroacetylacetone

Daryl L. Howard,[†] Henrik G. Kjaergaard,[*,¶] Jing Huang,[§] and Markus Meuwly[*,||]

Australian Synchrotron, 800, Blackburn Road, Clayton, Victoria 3168, Australia, Department of Chemistry, University of Otago, P.O. Box 56, Dunedin, New Zealand, Department of Chemistry, University of Copenhagen, Universitetsparken 5, DK-2100 Copenhagen, Danmark, Department of Pharmaceutical Science, University of Maryland, Baltimore, Department of Chemistry, University of Basel, Klingelbergstrasse 80, 4056 Basel Switzerland, and Department of Chemistry, Brown University, Providence (RI), USA

E-mail: hgk@chem.ku.dk; m.meuwly@unibas.ch

Abstract

The infrared and near infrared spectra of acetylacetone, acetylacetone-d_8 and hexafluoroacetylacetone are characterized from experiment and computations at different levels. In the fundamental region, the intramolecular hydrogen bonded OH-stretching transition is clearly observed as a very broad band with substantial structure and located at significantly lower frequency compared to common OH-stretching frequencies. There is no clear evidence for OH-stretching overtone transitions in the near infrared

*To whom correspondence should be addressed
[†]Australian Synchrotron, 800, Blackburn Road, Clayton, Victoria 3168, Australia
[‡]Department of Chemistry, University of Otago, P.O. Box 56, Dunedin, New Zealand
[¶]Department of Chemistry, University of Copenhagen, Universitetsparken 5, DK-2100 Copenhagen, Danmark
[§]Department of Pharmaceutical Science, University of Maryland, Baltimore
[||]Department of Chemistry, University of Basel, Klingelbergstrasse 80, 4056 Basel Switzerland
[⊥]Department of Chemistry, Brown University, Providence (RI), USA

region, which is dominated by the CH-stretching overtones of the methine and methyl CH bonds. From molecular dynamics (MD) simulations, with a potential energy surface previously validated for tunneling splittings, the infrared spectra are determined and used in assigning the experimentally measured ones. It is found that the simulated spectrum in the region associated with the proton transfer mode is exquisitely sensitive to the height of the barrier for proton transfer. Comparison of the experimental and the MD simulated spectra establishes that the barrier height is around 2.5 kcal/mol, which favourably compares with 3.2 kcal/mol obtained from high-level electronic structure calculations.

Introduction

Acetylacetone (AcAc) and hexafluoroacetylacetone (HFAA) are β-dicarbonyls which exist in two isomeric forms: the keto and enol tautomers shown in Figure 1a. The greater proportion of the enol form can be attributed to the resonance stabilization of the conjugated double bonds and to the stabilization provided by the intramolecular O–H$\cdots$O hydrogen bond. Increasing π electron delocalization may transform the H bond from an asymmetric O–H$\cdots$O pattern with a double well potential, to a symmetric O$\cdots$H$\cdots$O single well structure. If the π delocalization is complete, a symmetric C_{2v} structure is formed in which the C=C and C–C bonds, along with the C–O and C=O bonds, become equivalent and the H atom is shared equally between the two O atoms. A diagram of the interconversion process is shown in Figure 1b.

The thermodynamics of the keto-enol equilibrium of gas phase AcAc has been studied with temperature dependent nuclear magnetic resonance (NMR) spectroscopy.[1] The enol form is predominant with $\Delta H^{\circ}(\text{enol} \rightarrow \text{keto}) = 4.66 \pm 0.18$ kcal/mol and $\Delta S^{\circ} = 8.3$ cal/mol K^{-1}. The hydroxyl proton resonance full width at half maximum is approximately 16.7 Hz at 373 K, which is significantly broader than the $\sim$ 2 Hz line widths typical of the other proton resonances. The extra width of the hydroxyl proton resonance is indicative of its delocalization. The keto isomer was estimated to be about 4.1 to 4.3 kcal/mol higher in energy than the enol isomer from photoelectron[2] and ultraviolet[3] spectra. The gas phase abundance of the enol form of AcAc has been reported at various temperatures: 98% at 298 K from a ^{1}H NMR study,[1] 95% at 333 K and $\sim$ 60% at 503 K from infrared (IR) studies.[4]

AcAc is structurally related to its much more thoroughly characterized cousin malonaldehyde (MA, R=H in Figure 1) through substitution of the symmetrical H-atoms by methyl groups. Given that the methyl torsion can couple to the O–O stretch and hence to the proton transfer (PT) motion along the H–bond, it constitutes a more challenging problem than PT

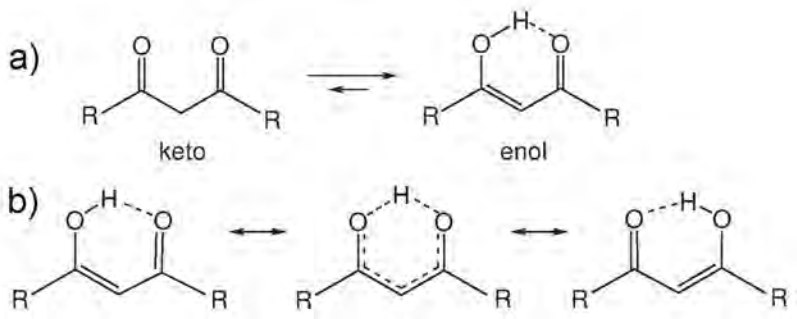

Figure 1: a) Keto-enol tautomerization in β-dicarbonyls. b) Interconversion of the enol form of a β-dicarbonyl. The transition state shown in the center has C_{2v} symmetry.

in MA. For MA, a number of IR spectra[5–8] and the ground state tunneling splitting[9,10] have been measured with high accuracy experimentally. A combined IR and Raman spectroscopy study of MA in supersonic jets and rare gas matrices recorded a tunneling splitting of 69 cm^{-1} with the OH-bend vibrationally excited.[11] Calculations at different levels of theory have been carried out to assign these spectra and to reproduce the splitting. In general, this requires fully dimensional dynamics simulations[12–17] performed on high level potential energy surfaces (PESs).[18]

Contrary to MA, less information about activation barriers, structures and possible tunneling splittings in AcAc is available. Even the question whether its ground state assumes an asymmetric (C_s) or a symmetric (C_{2v}) structure is still debated.[19–24] Neutron crystallography predicts that the ground state of AcAc has C_s symmetry.[19] Results from electron diffraction experiments are contradictory, suggesting either a C_s[20,21] or a C_{2v} structure.[23] The most recent study performed with ultrafast electron diffraction concluded that the lowest energy form of AcAc has C_s symmetry.[22] In general, electronic structure calculations find an asymmetric minimum energy structure with C_s symmetry for AcAc on the PESs excluding zero-point corrections,[25–30] while correcting for zero point vibrational energy lead to a slight preference of the C_{2v} minimum energy structure at the MP2/D95++** (for energies) and scaled HF/D95++** (for vibrations) level of theory[30] which can, however, not be compared

in quality to more recent[28] and present high-level calculations.

Conversely, high-resolution rotational spectra of AcAc and its singly substituted ^{13}C-isotopologues in the frequency ranges 2–26.5 GHz ($\sim$0.1–1 cm^{-1}) and 60–80 GHz ($\sim$2–3 cm^{-1}) lead to a structure with C_{2v} symmetry[24] possibly due to zero point vibration of the proton in systems with strong hydrogen bonds.[31–33] The double well potential in AcAc due to PT from one oxygen to another is responsible for the tunneling splitting.[34,35] Depending on whether or not the proton is constrained in the well will have a marked effect on the spectroscopy with respect to tunneling effects, thus isotopic substitution can be enlightening. To date only the microwave spectrum of the normal protonated isotopomer has been investigated,[24] and it would be informative to observe the microwave spectrum of a deuterated isotopomer of AcAc, where the tunneling splitting will be reduced due to the heavier isotope.

Several IR spectroscopic studies of AcAc are available in the vapor phase.[4,36–38] The OH–stretching transition is very broad, however is typically assigned in the region from 2750 cm^{-1} to 2800 cm^{-1}.[36,38] The only near infrared (NIR) investigation of AcAc was performed in the liquid phase in 1929 as part of a study regarding carbonyl overtones.[39] Other than a tentative assignment of a carbonyl overtone at 1.91 μm, no further transitions for AcAc were assigned.

Various experimental studies of hexafluoroacetylacetone (HFAA) have been performed including electron diffraction,[40,41] and IR spectroscopy[36,37] and microwave spectroscopy.[42] The microwave data shows that HFAA exists in a 'rigid' enolic C_s form, and it lacks doubling of rotational lines, indicating high effective barriers to the internal motions,[42] while the related molecule trifluoacetylacetone exhibits intermediate internal dynamics between AcAc and HFAA.[43] From gas phase electron diffraction studies it was concluded that HFAA exists as an enol tautomer with a planar symmetric ring and an O–H$\cdots$O angle close to 180°.[40,41]

The O···O distance was determined to be 2.551 Å[40] or 2.606 Å.[41] The symmetric ring conclusion has been refuted,[44] because such a structure having a nearly linear O–H···O angle should have only one minimum for its potential energy well and a smaller O···O distance of 2.3 Å is more likely (see, e.g., Ref.[45]). Alternatively, the symmetric structure based on the electron diffraction data has been interpreted as a superposition of two asymmetric structures.[46] High level electronic structure calculations on HFAA are demanding due to the extra computational cost associated with the six fluorine atoms and investigations have been limited.[26,44,46] The theoretical calculations yield structures analogous to AcAc, with an asymmetric C_s enol form as the most stable conformation.

The present work reports the vapor phase IR and NIR spectra of AcAc, AcAc-d_8, and HFAA. To assist in the interpretation of the experimental spectra, *ab initio*, anharmonic local mode oscillator calculations[47–49] and atomistic simulations are used.

Methods

Experiment

Liquid AcAc (Aldrich, >99%), AcAc-d_8 (fully deuterated AcAc, Cambridge Isotope Laboratories, 98% D) and HFAA (Merck-Schuchardt, 98%) were degassed with several freeze-pump-thaw cycles and dried with molecular sieves.

The IR spectra of gaseous AcAc, AcAc-d_8 and HFAA were recorded at 1 cm^{-1} resolution on a Perkin Elmer Spectrum BX FTIR spectrometer. Samples were contained in a 10 cm path length cell equipped with KBr windows. Both, the AcAc and AcAc-d_8 spectra were taken at 7 Torr vapour pressure and HFAA 10 Torr. The AcAc, AcAc-d_8 and HFAA spectra were measured at 291 K, 294 K and 295 K, respectively.

The conventional NIR spectra of AcAc and AcAc-d_8 were recorded with a Varian Cary 500 spectrophotometer which incorporated a 4.8 m path length White cell (Infrared Analysis, Inc.) fitted with Infrasil quartz windows. The spectrum of each sample was measured at 6 Torr vapor pressure and at 293 K. The spectrum of HFAA was recorded under the same conditions except at a pressure of 20 Torr. Background scans with an evacuated cell were subtracted from the sample spectra. A 0.2 OD neutral density filter was used as an attenuator in the reference beam path of the Cary 500.

AcAc and AcAc-d_8 were recorded with a photoacoustic spectrometer at pressures of 7 Torr and 8 Torr, respectively. Our photoacoustic spectrometer and the spectral calibration process has been described previously.[50,51] Briefly, a Coherent Innova Sabre argon ion laser running at all lines was used to pump a Coherent 890 titanium:sapphire laser. The wavelength is tuned with a three-plate birefringent filter which yields a laser line width of approximately 1 cm^{-1}. The photoacoustic cell contained a Knowles EK3133 microphone for detection of the photoacoustic signal. The corrosive nature of HFAA necessitated a low sample pressure in the photoacoustic cell to prevent damage to the microphone. The photoacoustic spectra of HFAA were recorded with a sample pressure of approximately 0.5 Torr. The photoacoustic signal of HFAA was enhanced by the addition of a buffer gas of 227 Torr argon to the photoacoustic cell.[52,53] All photoacoustic spectra were measured at 293 K.

Computational Methods

Anharmonic local mode calculations: The C_2 and C_{2v} structures of AcAc were optimized with the MP2/6-311++G(d,p) and CCSD(T)/cc-pVTZ methods using Gaussian09 and MOLPRO, respectively.[54,55] For the OH-stretching vibrations of AcAc and HFAA an anharmonic oscillator local mode model was used.[47,48] As usual, the OH-stretching oscillator is modelled

as a Morse oscillator.[49] The 1-dimensional PES and dipole moment surface for the OH-stretching coordinate were calculated at the CCSD(T)/cc-pVTZ level. The details of this model are given elsewhere.[49]

Intermolecular Interactions and Morphing: A detailed account of the Molecular Mechanics with Proton Transfer (MMPT) method has been given previously.[15,56–58] Briefly, MMPT uses parametrized three-dimensional potential energy surfaces (PESs) fitted to *ab initio* calculations at the MP2/6-311++G(d,p) level to describe the interactions within a general DH–A motif where D is the donor, H is the hydrogen and A is the acceptor atom. Together with a standard force field - here, CHARMM[59] is used - specific rules control how bonded interactions on the donor and acceptor side are switched on and off depending on the position of the transferring H-atom (DH–A or D–HA). To adapt the overall shape of the PES to topologically similar, but energetically different hydrogen bonding patterns - depending on the chemical environment of D and A - the PES can be "morphed".[60,61] Morphing can be a simple coordinate scaling or a more general coordinate transformation.

Table 1: The geometries of optimized (OPT) and transition state (TS) structures, together with the PT barrier ΔE for AcAc and MA calculated at the MP2/aug-cc-pVTZ level, which are used in the PES morphing. See text for details.

	AcAc		MA	
	OPT	TS	OPT	TS
R(Å)	2.53	2.36	2.56	2.36
r(Å)	1.01	1.20	1.00	1.20
θ(°)	17.9	10.8	19.4	10.6
ρ	0.17	0.5	0.15	0.5
d (Å)	0.31	0.22	0.33	0.22
ΔE (kcal/mol)	2.18		2.74	

For proton transfer in AcAc, the MMPT potential $V(R,\rho,d)$ depends on R, $\rho = (r\cos\theta - r_{\min})/(R - 2r_{\min})$ and $d = r\sin\theta$ where R is the O_1–O_2 distance, r is the O_1–H distance, and θ is the angle between $\vec{R}$ and $\vec{r}$ (see Fig. 2). The parameter $r_{\min} = 0.8$ Å is in principle

arbitrary but should be sufficiently small to cover the shortest possible D–H separations to ensure $\rho > 0$. The MMPT potential for AcAc is generated via PES morphing from that of MA,[15] since the PT motifs in the two molecules experience chemically similar environments. Morphing is achieved by modifying MMPT parameters and thus reshaping the interaction potentials, with reference data such as equilibrium structure and energy barrier provided by electronic structure calculations (Table 1). Different morphing schemes are tested and discussed in detail in the supplementary material. In the present work $V^{\mathrm{AcAc}}(R, \rho, d)$ and $V^{\mathrm{MA}}(R, \rho, d)$ are related through the following transformations:

$$V^{\mathrm{AcAc}}(R, \rho, d) = \lambda V^{\mathrm{MA}}(R - R_0, \rho, d) \tag{1}$$

with morphing parameters $\lambda = \frac{\Delta E^{\mathrm{AcAc}}}{\Delta E^{\mathrm{MA}}} = \frac{2.18\mathrm{kcal/mol}}{2.74\mathrm{kcal/mol}} = 0.796$ and $R_0 = R_{opt}^{\mathrm{MA}} - R_{opt}^{\mathrm{AcAc}} = 2.56$ Å-2.53 Å$= 0.03$ Å determined from comparing the PT barrier (ΔE) and the equilibrium donor-acceptor distance (R_{opt}) of AcAc and MA computed at the same level of theory (MP2/aug-cc-pVTZ). With such a morphing scheme information concerning the PT barrier height, and partly the PT barrier width as reflected in the O–O distance, are included. The entire set of parameters for $V(R, \rho, d)$ and comparison with those of MA are listed in the SI (Tables S2 and S3). Other force field parameters for all bonded and non-bonded interactions in AcAc are identical to those for MA, while the substituted methyl and trifluoromethyl groups are treated with existing CHARMM force field parameters.[59]

Infrared spectra and assignments from MD simulations: IR and power spectra are computed from suitable time correlation functions from MD simulations. More specifically, the total dipole moment $\vec{M}(t)$ was recorded along the MD trajectories and correlated over 2^{14} time origins to give the dipole-dipole correlation function $C(t)$

$$C(t) = \left\langle \vec{M}(t) \cdot \vec{M}(0) \right\rangle \tag{2}$$

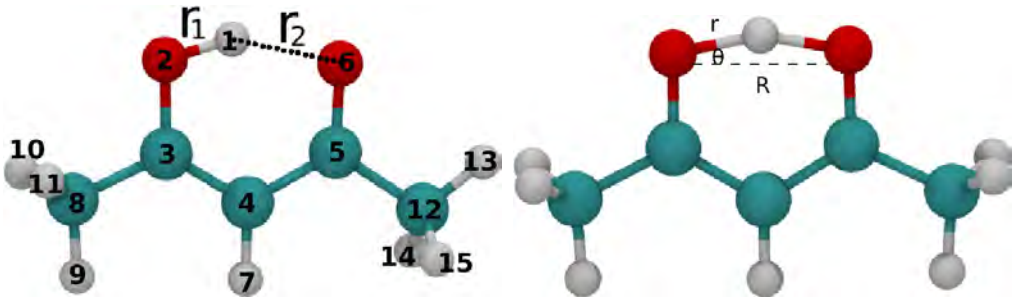

Figure 2: Equilibrium structure (left) and PT transition state structure (right) of AcAc, computed by MM force field. Atom types and internal coordinates (R,r and θ) for the MMPT potential are also labeled. See text for more details.

To suppress noise, a Blackman filter was used.[62] Then $C(\omega)$, the Fourier-Transform of $C(t)$, was weighted with the Boltzmann factors to give the IR spectrum $A(\omega)$

$$A(\omega) = \omega\{1 - \exp[-\hbar\omega/(k_B T)]\}C(\omega) \tag{3}$$

where k_B is the Boltzmann constant and T is the temperature.

MD trajectories also offer the possibility to determine power spectra corresponding to selected internal coordinates q. Such power spectra can be employed to assign spectroscopic features to motion along these coordinates and to analyze possible couplings between different internal coordinates. For this, the time series $q(t)$ is used to construct the correlation function $\langle q(t) \cdot q(0) \rangle$. The Fourier transform (see above) of this correlation function yields the power spectrum.

Results and Discussion

Molecular Geometries and Energies

The fully optimized geometry of the C_s and the C_{2v} structures of AcAc at the MP2 and CCSD(T)/cc-pVTZ level are compared with parameters from an electron diffraction (ED) experiment[22] in Table S4 (supporting information). Due to the weak scattering of the hydrogen atom, the O–H and H$\cdots$O distances and the O–H$\cdots$O angle were held at the B3LYP calculated values in the ED data.[22] The computed geometries are in good mutual agreement and agree well with experimentally determined structures which show some variation: the O$\cdots$O distances are 2.592 Å[22] and 2.547 Å respectively,[63] which compares favourably with our CCSD(T)/cc-pVTZ value of 2.55 Å. The C_s structure is significantly more stable than the C_{2v} structure by approximately 2.2 kcal/mol and 3.2 kcal/mol at the MP2/aug-cc-pVTZ and the CCSD(T)/cc-pVTZ levels, respectively. The energy differences can be considered as the classical barrier to PT. The relative structural degeneracy of the C_s and C_{2v} structures is 2:1, statistically favoring the C_s structure (Figure 1b) by $-RT\ln 2$ which is approximately 0.4 kcal/mol at 298 K. Hence, at the MP2 level of theory the C_s is more stable by $\approx$ 2.6 kcal/mol compared to the C_{2v} structure. Harmonic frequency calculations at this level of theory yield a zero-point vibrational energy (ZPVE) of 77.7 kcal/mol and 75.3 kcal/mol for the C_s and C_{2v} structures, respectively, which is a difference of 2.4 kcal/mol. At the MP2 level of theory it is therefore difficult to unambiguously assign the minimum energy structure to either C_s and C_{2v} symmetry, whereas the electronic energy difference of the CCSD(T) calculations favor the C_s structure, even with inclusion of the MP2 ZPVE difference to the CCSD(T) energies.

Methyl Groups: An evident structural difference between the C_s and C_{2v} structures is the orientation of the methyl group with the parent carbon labelled "12" in Figure 2. Hence, the torsion of this methyl group is coupled to the PT coordinate. In the transition state –

labelled TS2[28] the methyl groups eclipse one another (see Figure S1).

The MP2/aug-cc-pVTZ calculated energy difference between the TS2 and C_s structure, *i.e.*, the barrier to the methyl rotation, is 0.13 kcal/mol, in quite good agreement with the 0.27 kcal/mol obtained at the CCSD(T)/cc-pVTZ//MP2(FC)/cc-pVTZ level[28] and with microwave data at 0.163 kcal/mol.[24] Interestingly, the torsional barrier of the CH_3 group of acetone is considerably higher (0.76 kcal/mol).[64] Thus, the ring structure in AcAc must play a role in lowering the barrier to rotation of that methyl group. The C_s and TS2 enol forms of AcAc were calculated to have their OH–stretching vibrations separated by ≈ 500 cm^{-1}, which indicates that methyl torsion could lead to a broad OH-stretching band. In the force field treatment (vide infra) coupling between the CH_3 rotation and the H-transfer coordinate is not explicit. Nevertheless, the two degrees of freedom are coupled through stretching, bending and torsional terms in the overall force field.

The barrier for methyl rotation of the C8 methyl group (Figure 2) in AcAc is calculated to be 1.45 kcal/mol at the MP2(FC)/6-311G(d,p) level.[27] Methyl barrier heights of 0.45 kcal/mol and 1.17 kcal/mol were predicted based on inelastic neutron scattering measurements on solid AcAc[65] and in the range of 0.44–1.59 kcal/mol in more recent experiments on the enol tautomer.[19] The potential barriers of the enol tautomer were also sensitive to deuteration of the nonmethyl protons.[19] This is further indication of the coupling between the methyl rotation and PT. In contrast, the methyl potential of the keto tautomer was insensitive to these factors.

Equilibrium structures from the Reactive Force Field: The minimum and transition state (TS) structures calculated from the MMPT force field compare favorably with those from *ab initio* calculations at the MP2/aug-cc-pVTZ level (see Table 2). Differences in bond lengths and angles are within 0.02 Å and 3°, respectively. The energy difference between

the minimum (C_s) and TS (C_{2v}) structure is 2.35 kcal/mol, which is in good agreement with the MP2/aug-cc-pVTZ ab initio value of 2.17 kcal/mol. Also listed in Table 2 are the conformationally averaged geometries from 5 ns MD simulations in the gas phase. In such an ensemble averaged structure the proton is equally shared by the two oxygen atoms which corresponds to C_{2v} symmetry. This is not in conflict with a C_s minimum structure and ultrafast methods may be successful in detecting asymmetric structures.

Table 2: Comparison of selected bond lengths and angles of AcAc minimum and transition state obtained from *ab initio* MP2/aug-cc-pVTZ (QM) and force field (MMPT) optimizations. Also, the ensemble average from 5 ns MD simulations of gas phase AcAc is given.

	Min		TS		MD Aver.
	MMPT	QM	MMPT	QM	
O_1H_1 (Å)	1.009	1.006	1.199	1.202	1.306
O_2H_1 (Å)	1.590	1.601	1.199	1.202	1.304
O_1O_2 (Å)	2.536	2.528	2.350	2.362	2.518
$H_1O_1O_2$ (°)	15.86	17.93	11.27	10.76	15.03

Experimental Spectra

AcAc: The IR spectra of vapor phase AcAc and AcAc-d_8 are shown in Figure 3a. In both spectra the absorbance is low above 1700 cm^{-1}, so the absorbance scale in this region has been magnified in the figure to emphasize the structure relating mainly to the OH(OD)– and CH(CD)–stretching transitions. Hydrogen bonding can lead to very broad OH-stretching fundamental (ν_{OH})[66] and overtone bands.[67,68] The intensity of the ν_{OH} band of AcAc appears weak, however significant intensity is spread over a wide wavenumber region. The intramolecular H-bond is strong in AcAc and ν_{OH} is broad and lower in wavenumber than the ν_{CH} transitions. In the literature, ν_{OH} is typically assigned in the range of 2750 cm^{-1} to 2800 cm^{-1}.[36,38] However, we observe several transitions in the 2000–3300 cm^{-1} region.

The IR spectrum of AcAc-d_8 was closely examined for the small impurity of OH present in the compound, however no correspondence between the AcAc and AcAc-d_8 spectra in the ν_{OH} region was found. This is in contrast to findings for other examples with hydrogen impurities.[69] The ν_{OD} transition of AcAc-d_8 is more defined and narrower compared to the ν_{OH} band in AcAc.

The conventional NIR spectra of vapor phase AcAc and AcAc-d_8 are presented in Figure 4a. Relatively strong combination bands are present in the 4000–4600 cm^{-1} region of both isotopomers. The far wings of the more intense ν_{CH} transitions contribute to the sloping baseline at low wavenumber in the AcAc spectrum. The $\Delta v_{CH} = 2$ region is observed near 6000 cm^{-1}. The small CH impurities present in the AcAc-d_8 sample are apparent in the spectrum. The $\Delta v_{CH} = 2$ and 3 regions of AcAc and AcAc-d_8 are shown in Figures S2 and S3 in the supplementary information, respectively.

The photoacoustic spectra of AcAc and AcAc-d_8 are shown in Figures 5a and 5b, respectively. The slightly overlapping scans shown in each figure correspond to the various optics used in the Ti:sapphire laser. The intensity axis of each trace presented in the figures has been expanded to show the transitions clearly. For example, the AcAc $5\nu_{CH}$ transition is approximately an order of magnitude less intense than $4\nu_{CH}$.

HFAA: The IR spectrum of HFAA is shown in Figure 3b. Like the spectrum of AcAc, the ν_{OH} transition of HFAA is extremely broad and clearly contains many transitions. The values for ν_{OH} in HFAA has been given in the literature in the range from 2965 cm^{-1} to 3000 cm^{-1}.[36,37] However, just as for AcAc it is not possible to assign only one transition to the OH-stretching transition. The methine ν_{CH} transition is located at 3134 cm^{-1}, which is approximately 40 cm^{-1} higher than that in AcAc.

The conventional NIR spectrum of vapor phase HFAA is shown in Figure 4b. Its NIR spectrum is simpler than AcAc because the methyl CH transitions are absent. In the 4000–5000 cm^{-1} region, there is a quartet of peaks at 4049, 4233, 4405 and 4584 cm^{-1}. The peaks are approximately evenly separated by 180 cm^{-1}, and the intensity of the four peaks progressively drops with increasing wavenumber. In the 7000–8000 cm^{-1} region, a similar pattern of peaks is observed, however the spacing between them is not as regular. The pattern could be due to Fermi resonance, which is common in CH-stretching spectra of compounds such as CF_3H and CF_3CCH.[70]

The photoacoustic spectra of HFAA are shown in Figure 5c. In this wavenumber region, transitions from the OH– and methine CH–stretching oscillator, would be expected to contribute to the observed spectrum. The spectra are very simple, because transitions from the methyl CH oscillators are absent, and show no sign of an OH-stretching transition. There is no evidence for a Fermi resonance in the higher wavenumber region as it was in the 4000-9000 cm^{-1} region. The methine $4\nu_{CH}$ and $5\nu_{CH}$ transitions are dominant at 11841 cm^{-1} and 14527 cm^{-1}, respectively. The weak CH–stretching/bending combination band, $4\nu_{CH} + \delta\nu_{CH}$ is observed at 12898 cm^{-1}.

Apart from the tentative $2\nu_{OH}$ regions shown in Figure S4, higher overtone OH–stretching transitions were not observed in the photoacoustic spectra of AcAc and HFAA. It is apparent that the detection of the OH–stretching transition is not straightforward because the linewidth of the OH–stretching transitions is very broad, and the first overtone transition has a weak intensity.[49]

The Methyl CH-Stretching Regions: The methyl band profile of the CH–stretching overtone regions can be used as a guide to estimate the methyl torsional barrier height. If the barrier to methyl torsion is large, then the methyl group position is effectively fixed on the time

scale of the CH vibrations and two transitions are observed in its CH–stretching overtone spectrum corresponding to the in-plane and out-of-plane CH. If, on the other hand, the methyl torsional barrier is very low, there is effectively free rotation of the methyl group and a more complex spectrum is observed.[71–76]

The methyl CH–stretching region of AcAc-d_8 is much simpler than that of AcAc (see Fig. 4a and Supporting Information), as expected since in the AcAc-d_8 sample, a methyl group is most likely to have only one proton as an impurity. Thus facile CH coupling in the methyl group is removed and the spectra are simpler, revealing an in-plane and out-of-plane CH–stretching transition. The relative intensity of the out-of-plane to in-plane CH-stretching transitions is approximately 2:1, which to first order reflects the statistical weight of the oscillators.

The C_s structure of AcAc has two nonequivalent methyl groups. Thus the CH–stretching overtone spectra of the methyl groups will overlap and complicate their interpretation. In our spectra we are likely observing the transitions of the in- and out-of-plane CH bonds of the higher torsional barrier methyl group (parent carbon 8 in Figure 2). The lower barrier methyl group will have less structure in its spectrum and be less distinct.[76]

The $\Delta v_{\mathrm{CH}} = 4$ and 5 methyl CH-stretching regions of AcAc, labelled as $4\nu_{\mathrm{CH_3}}$ and $5\nu_{\mathrm{CH_3}}$, respectively, are shown in Figure 5a. In both overtone regions, the methyl band profile is essentially a two-peak structure representing the in- and out-of-plane CH oscillators, and based on this observation, we would expect that the methyl torsional barrier height is greater than 0.7 kcal/mol.[76] Our finding is in fair agreement with previously determined barrier heights of $\sim$ 0.4-1.6 kcal/mol in solid AcAc.[19,65]

The Methine CH-Stretching regions: The observed methine CH–stretching overtone transi-

Table 3: Observed methine CH–stretching overtone wavenumbers and local mode parameters (cm^{-1}) of acetylacetone and hexafluoroacetylacetone.

Δv	$\tilde{\nu}$(AcAc)	$\tilde{\nu}$ (HFAA)
2	6056	6150
3	8913	9047
4	11640	11841
5		14527
$\tilde{\omega}$	3205.7 ± 4.7	3243.0 ± 3.5
$\tilde{\omega}x$	59.0 ± 1.2	56.4 ± 0.7

tions of AcAc and HFAA and the local mode parameters obtained from the observed $\Delta v = 2$ to 5 transitions are presented in Table 3. The methine CH-stretching local mode frequency of HFAA is 40 cm^{-1} higher than that of AcAc, and its anharmonicity is slightly smaller. The small standard deviations in the local mode parameters indicate that the Morse oscillator is a good approximation for the methine CH oscillator.

Computational Vibrational Spectroscopy and the Barrier to H-Transfer

Direct contact with the experimental spectra analyzed above can be made from IR spectra determined from atomistic simulations. This is a powerful approach which has been successfully followed in previous work.[77–82]

IR spectra from Molecular Dynamics Simulations at Finite Temperature: The computed IR spectrum for AcAc from the 5 ns MD simulation in the gas phase is reported and compared with the experimental spectrum in Figure 6a. The simulated spectrum reproduces most experimentally observed features. Certain band positions could be improved by explicitly adjusting the corresponding force constants of the force field. However, this is not the primary aim in the present work. Improved intensities could be obtained with a more accurate dipole moment surface (DMS) instead of point charges. For protonated water dimer a full (15-)dimensional DMS[83] has been used in previous work together with MMPT/MD simula-

tions, which leads to improved IR intensities.[57] No such DMS is currently available for AcAc.

One advantage of MD simulations is that power spectra of individual vibrational motions can be used to assign the spectra. Table 4 reports the most relevant bands and assignments. The strong band at 1624 cm^{-1} in the IR spectrum of AcAc was previously assigned to either the CO stretching mode or the OH in-plane bending mode.[36,37,84,85] The power spectrum of the CO stretching vibration (Figure 6b) finds a single peak at 1602 cm^{-1} and clearly relates the experimentally observed band to the CO stretching band. It is noted that the lineshape of the CO-stretch vibration is not very well reproduced by the simulations. This is related to the fact that computing the IR spectrum from the Fourier transform of the dipole-autocorrelation function alone does not necessarily lead to realistic lineshapes. For this, additional factors such as the lifetimes of the transitions would need to be taken into account.[86] However, for comparing line positions the present approach is suitable.[87] The power spectra can also be employed to identify potentially coupled coordinates. For example, a peak at 520 cm^{-1} (the O–O vibration) is found in both OH stretching and OH bending modes, illustrating that these modes are coupled. Also, the CH_3 torsion is coupled to this mode and to a number of other motions. However, the CH_3 torsional spectrum does not line up exactly with the O–O vibration probably because the coordinate from which this spectrum was determined is coupled to other motions of the methyl group, such as a CCH bending motion. As already stated, no explicit coupling terms between different vibrational degrees of freedom are taken into account in the CHARMM force field although this would, in principle, be possible. This has been done because the focus in the present simulations is on the proton transfer mode which is represented by the dedicated MMPT-part of the force field.

The IR and associated power spectra for AcAc-d_8 are reported in Figures 7a and b, and those for HFAA in Figure S5 in the supplementary information. Similar to AcAc many features of the spectrum are reasonably well reproduced. However, one band observed around

Table 4: Comparison of selected IR frequencies, MD simulations and *ab initio* harmonic oscillator (HO) vibrational analysis at the MP2/aug-cc-pVTZ level. All frequencies are in cm^{-1}, and the assignments are based on the power spectra from MD simulations. The experimental frequency of OO vibration is taken from Ref.[88]

Exp.	MD	HO	Assignment
2000-3300	2000-3200	3013	OH stretching
1171	1180	1004	OH bending
510	520	374	OO vibration
1626	1602	1658	C=O stretching

1250 cm^{-1} in the AcAc-d_8 spectrum is not present in the computed spectrum. On the other hand, the region of primary interest in the present work associated with the D-transfer band together with the C-D stretches is realistically captured.

A more direct comparison with experiment is afforded by comparing the spectral features corresponding to the PT mode, see Figure 8. The MMPT force field used so far has a barrier height of 2.35 kcal/mol, and the OH-spectrum is centered around ~ 2600 cm^{-1}, see inset of Figure 6. This compares quite favourably with experiment and is further discussed below.

A sensitivity test for the PT barrier height and its influence on the spectrum in the OH-stretching region was carried out. For this, the same simulations were repeated with half (1.17 kcal/mol) and twice (4.70 kcal/mol) the MMPT-barrier height of 2.35 kcal/mol. The center of the band, as judged from the OH-stretching power spectrum reported in Figure 8, shifts to 2000 cm^{-1} and 3750 cm^{-1} for the low and high barrier, respectively. Hence from comparing the computed and experimentally observed spectral features in the region of the proton transfer region, a barrier for PT of ≈ 2.5 kcal/mol is inferred. This compares well with a barrier height of 3.2 kcal/mol from the present CCSD(T)/cc-pVTZ calculations. The pronounced features in the experimental spectrum (purple) around 3000 cm^{-1} correspond to the C-H stretching vibrations which are not present in the O-H power spectrum. It is thus concluded that the H-transferring part of the IR spectrum is sensitive to the barrier height

which can be qualitatively extracted from such an analysis.

The power spectra of the OH-stretching are very broad and spread from 2000 cm^{-1} to 3200 cm^{-1}, emphasizing the very anharmonic nature of the OH stretching PT-mode which agrees with observations in the gas phase IR spectrum.[28,36] This is further illustrated by the IR spectra of the deuterated isotopomers of AcAc computed from MD simulations in gas phase (see Fig. S5 in the SI). Deuterating the transferring hydrogen shifts this broad band to lower frequencies. The simulations suggest that replacing the CH_3 groups by CD_3 leaves the shape of the OH-stretching band largely unaffected. This is established when comparing the OH- and OD-stretching regions in Figures 6 and 7.

Previous computational work employed reduced-dimensionality quantum dynamics simulations and found considerably narrower and stronger OH stretching bands.[28,88] For example, density matrix evolution simulations at 300 K found the asymmetric OH stretching band centered at 2500 cm^{-1} and to spread from 2300 cm^{-1} to 2800 cm^{-1}.[88] Low-temperature (1 K) MD simulations with the MMPT force field lead to a strong OH-stretching band at 2728 cm^{-1} (see Figure S7 in the SI), which should be amenable to matrix isolation spectroscopy at very low temperature. The OH bending modes are at 1180 cm^{-1}, which corresponds to the experimentally measured strong band at 1171 cm^{-1} by de-convoluted IR spectra.[38]

To further help explain the observed low intensity of the OH-stretching overtone transitions, the wavenumber and intensity of the OH-stretching vibration in AcAc has been calculated assuming a 1D local mode anharmonic oscillator. The CCSD(T)/cc-pVTZ calculated local mode parameters as well as the wavenumber and oscillator strength of the OH-stretching transitions are given in Table S7. The local mode parameters are consistent with a strong hydrogen bond, although the double well nature of the potential likely adds uncertainty to these values. The CCSD(T) AO calculation the $2\nu_{OH}$ region is predicted around 5200 cm^{-1}

with an intensity about 2 orders of magnitude weaker than the fundamental transition. This combined with the very broad nature of the OH-stretching transition as seen in the fundamental spectrum and in the MD simulation makes it unlikely that we can make clear observations of this transition.

Conclusions

The IR and NIR spectra of acetylacetone, acetylacetone-d_8, and hexafluoroacetylacetone were investigated from 600 to 14000 cm^{-1}. Geometry optimizations of the ground state and the transition state structures of AcAc at the CCSD(T)/cc-pVTZ level yield an electronic energy difference of approximately 3 kcal/mol favoring the C_s structure.

The fundamental OH-stretching band is observed as a very broad band redshifted relative to usual OH-stretching transitions. Higher overtone OH-stretching transitions were not found in either AcAc or HFAA, likely due to a combination of the expected weak and very broad overtone transitions. A progression of methine CH-stretching transitions were observed in all molecules, with the CF_3 groups of HFAA found to slightly blueshift relative to ν_{CH}.

IR and power spectra from atomistic simulations reproduce most experimentally recorded features and clearly assign the ν_{OH} proton transfer (PT) mode to the weak and broad band experimentally observed in the 2000-3300 cm^{-1} region. Furthermore, location of this band was found to sensitively depend on the barrier for PT from which a barrier for proton transfer of $\approx$ 2.5 kcal/mol is inferred. Therefore, combining experiment and atomistic simulations allowed us to estimate the barrier for proton transfer through comparison of the power spectrum and spectroscopic signature in the OH-stretching region in AcAc.

Acknowledgments

We thank the Marsden Fund administered by the Royal Society of New Zealand for support and the Lasers and Applications Research Theme at the University of Otago for use of their computer facilities. HGK thanks the Danish Council for Independent Research - Natural Sciences for financial support. The research of MM is supported by the Swiss National Science Foundation through projects 200020-132406 and the NCCR MUST, which is gratefully acknowledged.

Supporting Information Available: Three tables of optimized structures of AcAc. TS2 structure and detailed spectra of the $\Delta v_{\mathrm{CH}} = 2$ and 3 regions of AcAc and AcAc-d_8 and the $\Delta v_{\mathrm{OH}} = 2$ region of AcAc, AcAc-d_8 and HFAA. Comparison of different morphing schemes and the resulting MMPT parameters. Additional computed IR spectra from MD simulations. This material is available free of charge via the Internet at http://pubs.acs.org.d

References

(1) Folkendt, M. M.; Weiss-Lopez, B. E.; Chauvel, J. P.; True, N. S. Gas-Phase ^{1}H NMR Studies of Keto-Enol Tautomerism of Acetylacetone, Methyl Acetoacetate and Ethyl Acetoacetate. *J. Phys. Chem.* **1985**, *89*, 3347–3352.

(2) Hush, N. S.; Livett, M. K.; Peel, J. B.; Willett, G. D. Variable-Temperature Ultraviolet Photoelectron Spectroscopy of the Keto-Enol Tautomers of Pentane-2,4-dione. *Aust. J. Chem.* **1987**, *40*, 599–609.

(3) Nakanishi, H.; Morita, H.; Nagakura, S. Electronic structures and spectra of the keto and enol forms of acetylacetone. *Bull. Chem. Soc. Jpn.* **1977**, *50*, 2255–2261.

(4) Funck, E.; Mecke, E. In *Hydrogen Bonding*; Hadži, D., Ed.; Hydrogen Bonding, Pergamon: New York, 1959; pp 433–441.

(5) Smith, Z.; Wilson, E. B. The infrared spectrum of gaseous malonaldehyde (3-hydroxy-2-propenal). *Spectrochim. Acta A* **1983**, *39*, 1117–1129.

(6) Firth, D. W.; Barbara, P. F.; Trommsdorf, H. P. Matrix Induced Localization of Proton Tunneling in Malonaldehyde. *Chem. Phys.* **1989**, *136*, 349–360.

(7) Chiavassa, T.; Roubin, R.; Piazzala, L.; Verlaque, P.; Allouche, A.; Marinelli, F. Experimental and Theoretical-Studies of Malonaldehyde - Vibrational Analysis of a Strongly Intramolecularly Hydrogen-Bonded Compound. *J. Phys. Chem.* **1992**, *96*, 10659–10665.

(8) Duan, C.; Luckhaus, D. High Resolution IR-Diode Laser Jet Spectroscopy of Malonaldehyde. *Chem. Phys. Lett.* **2004**, *391*, 129–133.

(9) Baughcum, S. L.; Duerst, R. W.; Rowe, W. F.; Smith, Z.; Wilson, E. B. Microwave Spectroscopic Study Of Malonaldehyde (3-Hydroxy-2-Propenal) .2. Structure, Dipole-Moment, and Tunneling. *J. Am. Chem. Soc.* **1981**, *103*, 6296–6303.

(10) Firth, D. W.; Beyer, K.; Dvorak, M. A.; Reeve, S. W.; Grushow, A.; Leopold, K. R. Tunable far infrared spectroscopy of malonaldehyde. *J. Chem. Phys.* **1991**, *94*, 1812–1819.

(11) Luttschwager, N. O. B.; Wassermann, T. N.; Coussan, S.; Suhm, M. A. Periodic bond breaking and making in the electronic ground state on a sub-picosecond timescale: OH bending spectroscopy of malonaldehyde in the frequency domain at low temperature. *Phys. Chem. Chem. Phys.* **2010**, *12*, 8201.

(12) Viel, A.; Coutinho-Neto, M. D.; Manthe, U. The ground state tunneling splitting and

the zero point energy of malonaldehyde: A quantum Monte Carlo determination. *J. Chem. Phys.* **2007**, *126*, 024308.

(13) Hazra, A.; Skone, J. H.; Hammes-Schiffer, S. Combining the nuclear-electronic orbital approach with vibronic coupling theory: Calculation of the tunneling splitting for malonaldehyde. *J. Chem. Phys.* **2009**, *130*, 054108.

(14) Schroder, M.; Gatti, F.; Meyer, H.-D. Theoretical studies of the tunneling splitting of malonaldehyde using the multiconfiguration time-dependent Hartree approach. *J. Chem. Phys.* **2011**, *134*, 234307.

(15) Yang, Y.; Meuwly, M. A Generalized Reactive Force Field for Nonlinear Hydrogen Bonds: Hydrogen Dynamics and Transfer in Malonaldehyde. *J. Chem. Phys.* **2010**, *133*, 064503.

(16) Hammer, T.; Manthe, U. Intramolecular proton transfer in malonaldehyde: Accurate multilayer multi-configurational time-dependent Hartree calculations. *J. Chem. Phys.* **2011**, *134*, 224305.

(17) Huang, J.; Buchowiecki, M.; Nagy, T.; Vanicek, J.; Meuwly, M. Kinetic isotope effect in malonaldehyde from path integral Monte Carlo simulations. *PCCP* **2014**, *16*, 204–211.

(18) Wang, Y.; Braams, B. J.; Bowman, J. M.; Carter, S.; Tew, D. P. Full-dimensional quantum calculations of ground-state tunneling splitting of malonaldehyde using an accurate *ab initio* potential energy surface. *J. Chem. Phys.* **2008**, *128*, 224314.

(19) Johnson, M. R.; Jones, N. H.; Geis, A.; Horsewill, A. J.; Trommsdorff, H. P. Structure and dynamics of the keto and enol forms of acetylacetone in the solid state. *J. Chem. Phys.* **2002**, *116*, 5694–5700.

(20) Lowrey, A. H.; George, C.; D'Antonio, P.; Karle, J. Structure of Acetylacetone by Electron Diffraction. *J. Am. Chem. Soc.* **1971**, *93*, 6399–6403.

(21) Andreassen, A. L.; Bauer, S. H. Structures of acetylacetone, trifluoroacetylacetone, and trifluoracetone. *J. Mol. Struct.* **1972**, *12*, 381–403.

(22) Srinivasan, R.; Feenstra, J. S.; Park, S. T.; Xu, S.; Zewail, A. H. Direct Determination of Hydrogen-Bonded Structures in Resonant and Tautomeric Reactions Using Ultrafast Electron Diffraction. *J. Am. Chem. Soc.* **2004**, *126*, 2266–2267.

(23) Iijima, K.; Ohnogi, A.; Shibata, S. The molecular structure of acetylacetone as studied by gas-phase electron diffraction. *J. Mol. Struct.* **1987**, *156*, 111–118.

(24) Caminati, W.; Grabow, J. U. The C_{2v} structure of enolic acetylacetone. *J. Am. Chem. Soc.* **2006**, *128*, 854–857.

(25) Bauer, S. H.; Wilcox, C. F. On malonaldehyde and acetylacetone: are theory and experiment compatible? *Chem. Phys. Lett.* **1997**, *279*, 122–128.

(26) Sliznev, V. V.; Lapshina, S. B.; Girichev, G. V. *Ab Initio* Structure Investigation of the Enol Forms of β-Diketones $RCOCH_2COR$ (R=H, CH_3, CF_3). *J. Struct. Chem.* **2002**, *43*, 47–55.

(27) Matanović, I.; Došlić, N.; Mihalić, Z. Exploring the potential energy surface for proton transfer in acetylacetone. *Chem. Phys.* **2004**, *306*, 201–207.

(28) Matanović, I.; Došlić, N. Infrared Spectroscopy of the Intramolecular Hydrogen Bond in Acethylacetone: A Computational Approach. *J. Phys. Chem. A* **2005**, *109*, 4185–4194.

(29) Campomanes, P.; Menéndez, M. I.; Sordo, T. L. Resonance assisted hydrogen bonding and dynamic mechanism for crystal disorder in the enolic form of acetylacetone: a theoretical analysis. *J. Mol. Struct. (THEOCHEM)* **2005**, *713*, 59–63.

(30) Dannenberg, J. J.; Rios, R. Theoretical Study of the Enolic Forms of Acetylacetone. How Strong is the H-Bond? *J. Phys. Chem.* **1994**, *98*, 6714–6718.

(31) Asmis, K. R.; Yang, Y.; Santambrogio, G.; Brümmer, M.; Roscioli, J. R.; McCunn, L. R.; Johnson, M. A.; Kühn, O. Gas-phase infrared spectroscopy and multidimensional quantum calcaultions of the protonated ammonium dimer $(N_2H_7)^+$. *Angew. Chem. Int. Ed.* **2007**, *46*, 8691–8694.

(32) Yang, Y.; Kühn, O.; Santambrogio, G.; Goebbert, D. J.; Asmis, K. R. Vibrational signatures of Hydrogen bonding in the protonated ammonia clusters NH4+(NH3)1-4. *J. Chem. Phys.* **2008**, *129*, 224302.

(33) Yang, Y.; Kühn, O. *Z. Phys. Chem.* **2008**, *222*, 1375–1387.

(34) Hinsen, K.; Roux, B. Potential of mean force and reaction rates for proton transfer in acetylacetone. *J. Chem. Phys.* **1997**, *106*, 3567–3577.

(35) Mavri, J.; Grdadolnik, J. Proton Potential in Acetylacetone. *J. Phys. Chem. A* **2001**, *105*, 2039–2044.

(36) Ogoshi, H.; Nakamoto, K. Normal-Coordinate Analyses of Hydrogen-Bonded Compounds. V. The Enol Forms of Acetylacetone and Hexafluoroacetylacetone. *J. Chem. Phys.* **1966**, *45*, 3113–3120.

(37) Tayyari, S. F.; Zeegers-Huyskens, T.; Wood, J. L. Spectroscopic study of hydrogen bonding in the enol form of β-diketones–II. Symmetry of the hydrogen bond. *Spectrochim. Acta Part A* **1979**, *35*, 1289–1295.

(38) Tayyari, S. F.; Milani-nejad, F. Vibrational assignment of acetylacetone. *Spectrochim. Acta Part A* **2000**, *56*, 2679–2691.

(39) Ellis, J. W. The Near Infra-Red Absorption Spectra of Some Aldehydes, Ketones, Esters and Ethers. *J. Am. Chem. Soc.* **1929**, *51*, 1384–1394.

(40) Andreassen, A. L.; Zebelman, D.; Bauer, S. H. Hexafluoroacetylacetone and hexafluoroacetic anhydride. *J. Am. Chem. Soc.* **1971**, *93*, 1148–1152.

(41) Iijima, K.; Tanaka, Y.; Onuma, S. Internal rotation of trifluoromethyl groups in hexafluoroacetylacetone. *J. Mol. Struct.* **1992**, *268*, 315–318.

(42) Evangelisti, L.; Tang, S.; Velino, B.; Guilano, B. M.; Melandri, S.; Caminati, W. Hexafluoroacetylacetone: A 'rigid' molecule with an enolic C_s shape. *Chem. Phys. Lett.* **2009**, *473*, 247–250.

(43) Favero, L. B.; Evangelisti, L.; Velino, B.; Caminati, W. Morphing the Internal Dynamics of Acetylacetone by $CH_3 \rightarrow CF_3$ Substitutions. The Rotational Spectrum of Trifluoroacetylacetone. *J. Phys. Chem. A* **2014**, *118*, 4243–4248.

(44) Buemi, G. Ab initio DFT study of the hydrogen bridges in hexafluoro-acetylacetone, trifluoroacetylacetone and some 3-substituted derivatives. *J. Mol. Struct. (Theochem)* **2000**, *499*, 21–34.

(45) Emsley, J. The Composition, Structure and Hydrogen Bonding of the β-Diketones. *Struct. Bond.* **1984**, *57*, 147–191.

(46) Tayyari, S. F.; Milani-Nejad, F.; Rahemi, H. Structure and vibrational spectra of the enol form of hexafluoro-acetylacetone. A density functional theoretical study. *Spectrochimica Acta Part A* **2002**, *58*, 1669–1679.

(47) Henry, B. R. The Local Mode Model and Overtone Spectra: A Probe of Molecular Structure and Conformation. *Acc. Chem. Res.* **1987**, *20*, 429–435.

(48) Kjaergaard, H. G.; Yu, H.; Schattka, B. J.; Henry, B. R.; Tarr, A. W. Intensities in local mode overtone spectra: Propane. *J. Chem. Phys.* **1990**, *93*, 6239–6248.

(49) Howard, D. L.; Jørgensen, P.; Kjaergaard, H. G. Weak Intramolecular Interactions in Ethylene Glycol Identified by Vapor Phase OH–Stretching Overtone Spectroscopy. *J. Am. Chem. Soc.* **2005**, *127*, 17096–17103.

(50) Henry, B.; Kjaergaard, H.; Niefer, B.; Schattka, B.; Turnbull, D. The local mode model and recent advances in laser-based photoacoustic spectroscopy. *Can. J. Appl. Spect.* **1993**, *38*, 42–50.

(51) Rong, Z.; Kjaergaard, H. G. Internal Methyl Rotation in the CH Stretching Overtone Spectra of ortho-, meta-, and para-Xylene. *J. Phys. Chem. A* **2002**, *106*, 6242–6253.

(52) Wake, D. R.; Amer, N. M. The dependence of an acoustically nonresonant optoacoustic signal on pressure and buffer gases. *Appl. Phys. Lett.* **1979**, *34*, 379–381.

(53) Schattka, B. J.; Turnbull, D. M.; Kjaergaard, H. G.; Henry, B. R. Dependence of an Acoustically Nonresonant Intracavity Photoacoustic Signal on Sample and Buffer Gas Pressure. *J. Phys. Chem.* **1995**, *99*, 6327–6332.

(54) Frisch, M. J. et al. Gaussian 09, Revision A.02. Gaussian, Inc., Wallingford, CT, 2009.

(55) Werner, H.-J. et al. MOLPRO, version 2002.6, a package of ab initio programs. 2003.

(56) Lammers, S.; Lutz, S.; Meuwly, M. Reactive Force Fields for Proton Transfer Dynamics. *J. Comput. Chem.* **2008**, *29*, 1048–1063.

(57) Lammers, S.; Meuwly, M. Investigating the relationship between infrared spectra of shared protons in different chemical environments: A comparison of protonated Diglyme and protonated water dimer. *J. Phys. Chem. A* **2007**, *111*, 1638–1647.

(58) Lutz, S.; Tubert-Brohman, I.; Yang, Y.; Meuwly, M. Water-assisted proton transfer in ferredoxin I. *J. Biol. Chem.* **2011**, *286*, 23679–23687.

(59) MacKerell, J. A. D. et al. All atom empirical potential for molecular modeling and dynamics studies of proteins. *J. Phys. Chem. B* **1998**, *102*, 3586–3616.

(60) Bowman, J. M.; Gazdy, B. A simple method to adjust potential energy surfaces: Application to HCO. *J. Chem. Phys.* **1991**, *94*, 816–817.

(61) Meuwly, M.; Hutson, J. M. Morphing *ab initio* potentials: A systematic study of Ne–HF. *J. Chem. Phys.* **1999**, *110*, 8338–8347.

(62) Allen, M. P.; Tildesley, D. J. *Computer Simulation of Liquids*; Clarendon Press, Oxford, 1987.

(63) Boese, R.; Antipin, M. Y.; Bläser, D.; Lyssenko, A., Konstantin Molecular Crystal Structure of Acetylacetone at 210 and 110 K: Is the Crystal Disorder Static or Dynamic? *J. Phys. Chem. B* **1998**, *102*, 8654–8660.

(64) Vacherand, J. M.; Vaneijck, B. P.; Burie, J.; Demaison, J. The Rotational Spectrum of Acetone - Internal-Rotation and Centrifugal Distortion Analysis. *J. Mol. Spectrosc.* **1986**, *118*, 355–362.

(65) Horsewill, A. J.; Alsanoosi, A. M.; Carlile, C. J. Methyl tunnelling in acetylacetone. *J. Phys. C* **1987**, *20*, L869–L874.

(66) Pimentel, G. C.; McClellan, A. L. *The Hydrogen Bond*; W. H. Freeman: San Francisco, 1960.

(67) Howard, D. L.; Kjaergaard, H. G. Influence of Intramolecular Hydrogen Bond Strength on OH-Stretching Overtones. *J. Phys. Chem. A* **2006**, *110*, 10245–10250.

(68) Cheng, Y.-L.; Chen, Y., Hui; Takahashi, K. Theoretical Calculation of the OH Vibrational Overtone Spectra of 1-n Alkane Diols ($n = 2 - 4$): Origin of Disappearing Hydrogen-Bonded OH Peak. *J. Phys. Chem.* **2011**, *115*, 5641–5653.

(69) Kjaergaard, H. G.; Turnbull, D. M.; Henry, B. R. Intensities in CH– and CD–stretching overtones in 1,3–butadiene and 1,3–butadiene–d_6. *J. Chem. Phys.* **1993**, *99*, 9438–9452.

(70) Quack, M. Spectra and Dynamics of Coupled Vibrations in Polyatomic Molecules. *Annu. Rev. Phys. Chem.* **1990**, *41*, 839–874.

(71) Zhu, C.; Kjaergaard, H.; Henry, B. CH-stretching overtone spectra and internal methyl rotation in 2,6-difluorotoluene. *J. Chem. Phys.* **1997**, *107*, 691–701.

(72) Kjaergaard, H.; Turnbull, D.; Henry, B. Methyl versus aryl CH and CD stretching overtone intensities in the vapor phase spectra of toluenes. *J. Phys. Chem. A* **1997**, *101*, 2589–2596.

(73) Kjaergaard, H.; Turnbull, D.; Henry, B. Deuterium isotope effects on the CH stretching overtone spectrum of toluene-alpha-d(1). *J. Phys. Chem. A* **1998**, *102*, 6095–6100.

(74) Kjaergaard, H. G.; Henry, B. R.; Tarr, A. W. Intensities in local mode overtone spectra of dimethyl ether and acetone. *J. Chem. Phys.* **1991**, *94*, 5844–5854.

(75) Kjaergaard, H.; Rong, Z.; McAlees, A.; Howard, D.; Henry, B. Internal methyl rotation in the CH stretching overtone spectra of toluene-alpha-d(2), -alpha-d(1), and -d(0). *J. Phys. Chem. A* **2000**, *104*, 6398–6405.

(76) Rong, Z.; Howard, D. L.; Kjaergaard, H. G. Effect of the Methyl Internal Rotation Barrier Height on CH–Stretching Overtone Spectra. *J. Phys. Chem. A* **2003**, *107*, 4607–4611.

(77) Merchant, K. A.; Noid, W. G.; Thompson, D. E.; Akiyama, R.; Loring, R. F.; Fayer, M. D. Structural assignments and dynamics of the A substates of MbCO: spectrally resolved vibrational echo experiments and molecular dynamics simulations. *J. Phys. Chem. B* **2003**, *107*, 4–7.

(78) Nutt, D.; Meuwly, M. Theoretical investigation of infrared spectra and pocket dynamics of photodissociated carbonmonoxy myoglobin. *Biophys. J.* **2003**, *85*, 3612–3623.

(79) Nutt, D.; Meuwly, M. CO migration in native and mutant myoglobin: Atomistic simulations for the understanding of protein function. *Proc. Natl. Acad. Sci.* **2004**, *101*, 5998–6002.

(80) Lutz, S.; Nienhaus, K.; Nienhaus, G. U.; Meuwly, M. Pocket Dynamics of Photodissociated Carbonmonoxy Neuroglobin. *J. Phys. Chem. B* **2009**, *113*, 15334.

(81) Nienhaus, K.; Lutz, S.; Meuwly, M.; Nienhaus, G. U. Structural Identification of Spectroscopic Substates in Neuroglobin. *Chem. Phys. Chem.* **2010**, *11*, 119.

(82) Lee, M. W.; Carr, J. K.; Göllner, M.; Hamm, P.; Meuwly, M. 2D IR Spectra of Cyanide in Water Investigated by Molecular Dynamics Simulations. *J. Chem. Phys.* **2013**, *139*, 054506.

(83) Huang, S.; Braams, B. J.; Bowman, J. M. Ab initio potential energy and dipole moment surfaces for $H_5O_2^+$. *J. Chem. Phys.* **2005**, *122*, 044308.

(84) Bratoz, S.; Hadzi, D.; Rossmy, G. The infra-red absorption bands associated with the chelate ring in some unsaturated hydroxycarbonyl compounds. *Trans. Faraday Soc.* **1956**, *52*, 464–470.

(85) Tayyari, S. F.; Zeegers-Huyskens, T.; Wood, J. L. Spectroscopic study of hydrogen bonding in the enol form of β-diketones-I. Vibrational assignment and strength of the bond. *Spectrochim. Acta A* **1979**, *39*, 1265–1272.

(86) Cazade, P. A.; Bereau, T.; Meuwly, M. Computational two-dimensional infrared spectroscopy without maps: N-methylacetamide in water. *J. Phys. Chem. B* **2014**, *in print*.

(87) Berens, P.; K., W. *J. Chem. Phys.* **1981**, *74*, 4872–4882.

(88) Mavri, J.; Grdadolnik, J. Proton Transfer Dynamics in Acetylacetone: A Mixed Quantum-Classical Simulation of Vibrational Spectra. *J. Phys. Chem. A* **2001**, *105*, 2045–2051.

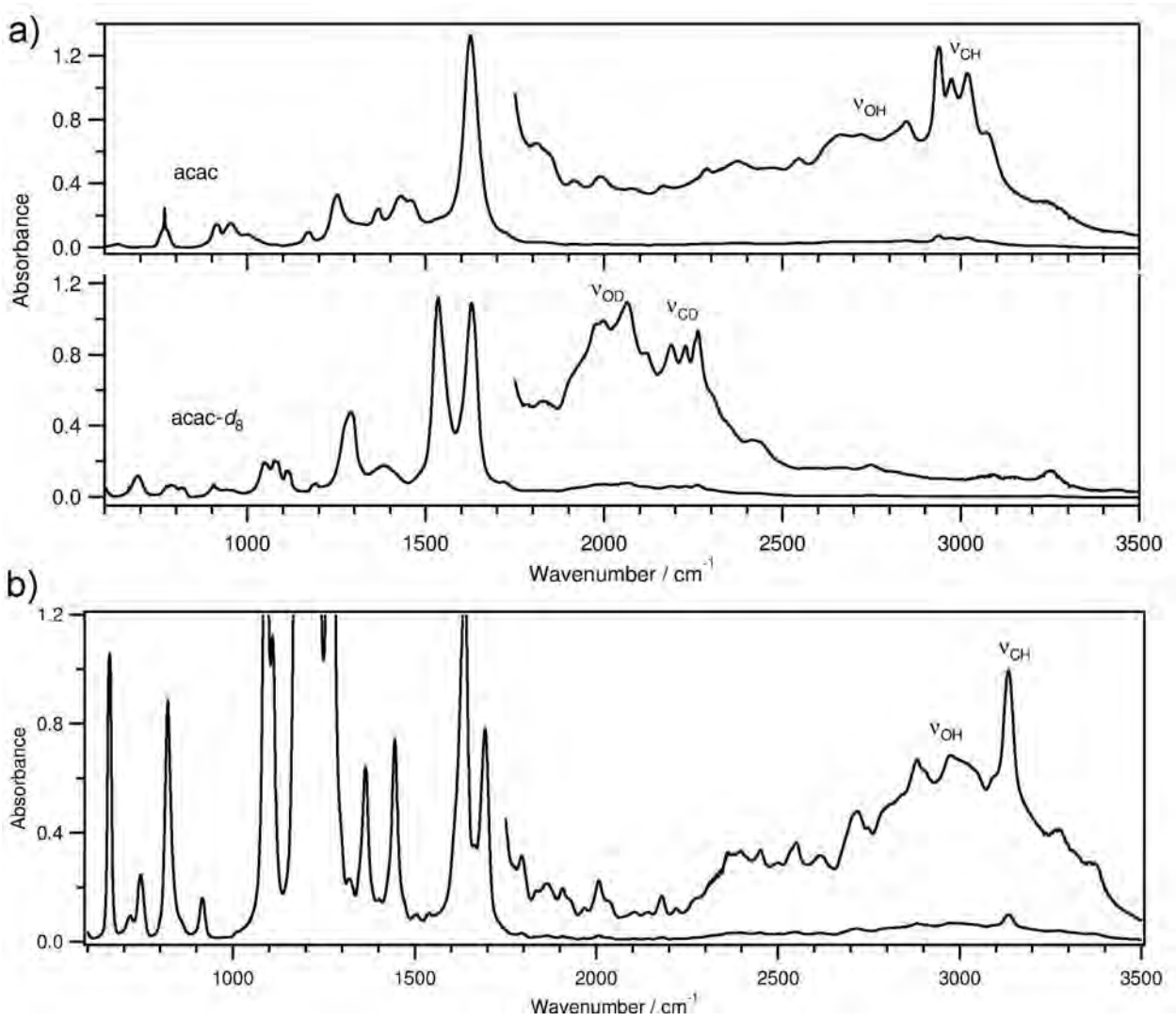

Figure 3: a) Experimental IR spectra of vapor phase AcAc (top) and AcAc-d_8. Both spectra were recorded at a pressure of 7 Torr and with a 10 cm path length. The AcAc and AcAc-d_8 spectra were recorded at 291 K and 294 K, respectively. b) IR spectrum of vapor phase hexafluoroacetylacetone recorded at a pressure of 10 Torr and 10 cm path length at 295 K. The ordinates of the high wavenumber region of each spectrum are expanded to reveal more detail.

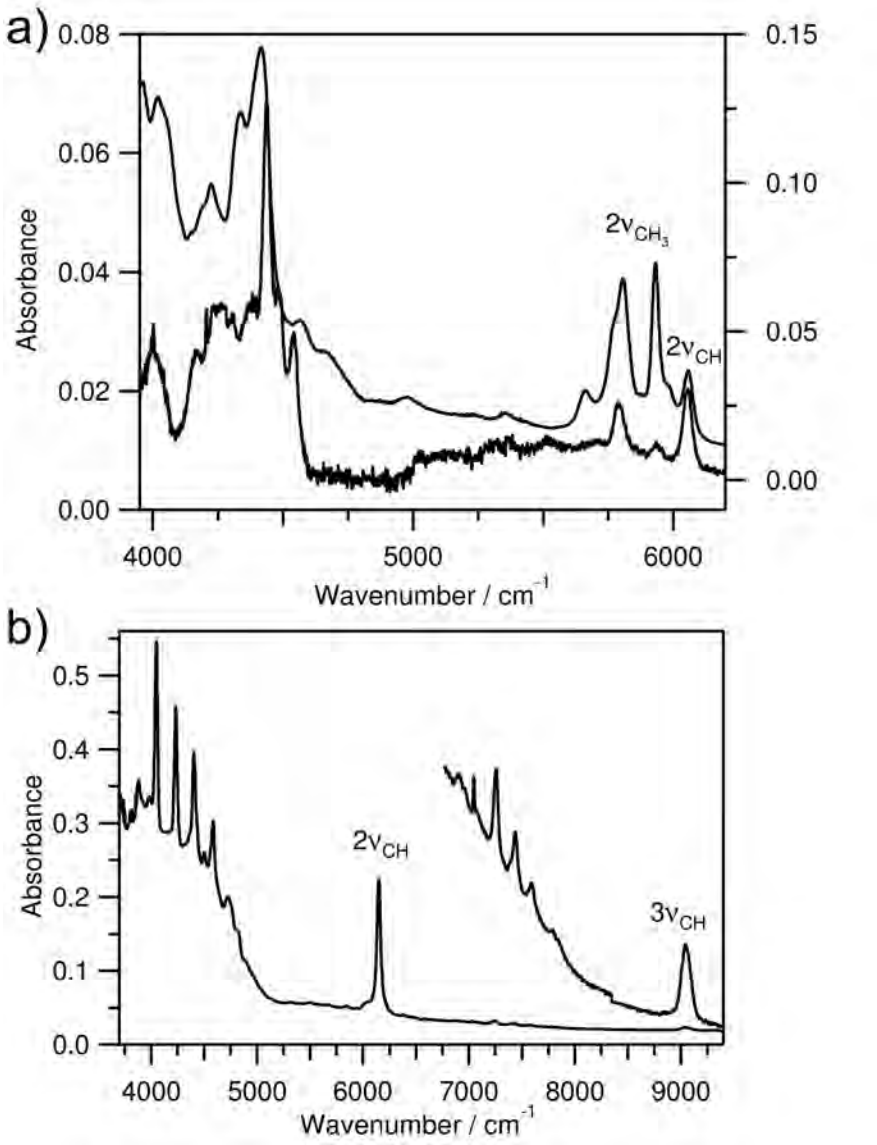

Figure 4: a) Vapor phase NIR spectra of AcAc (top) and AcAc-d_8. Both spectra were recorded at a pressure of 6 Torr, 294 K and with a 4.8 m path length. The left ordinate corresponds to the AcAc-d_8 spectrum. b) Vapor phase hexafluoroacetylacetone recorded at a pressure of 20 Torr, 293 K and with a 4.8 m path length. The high frequency region is expanded for more detail.

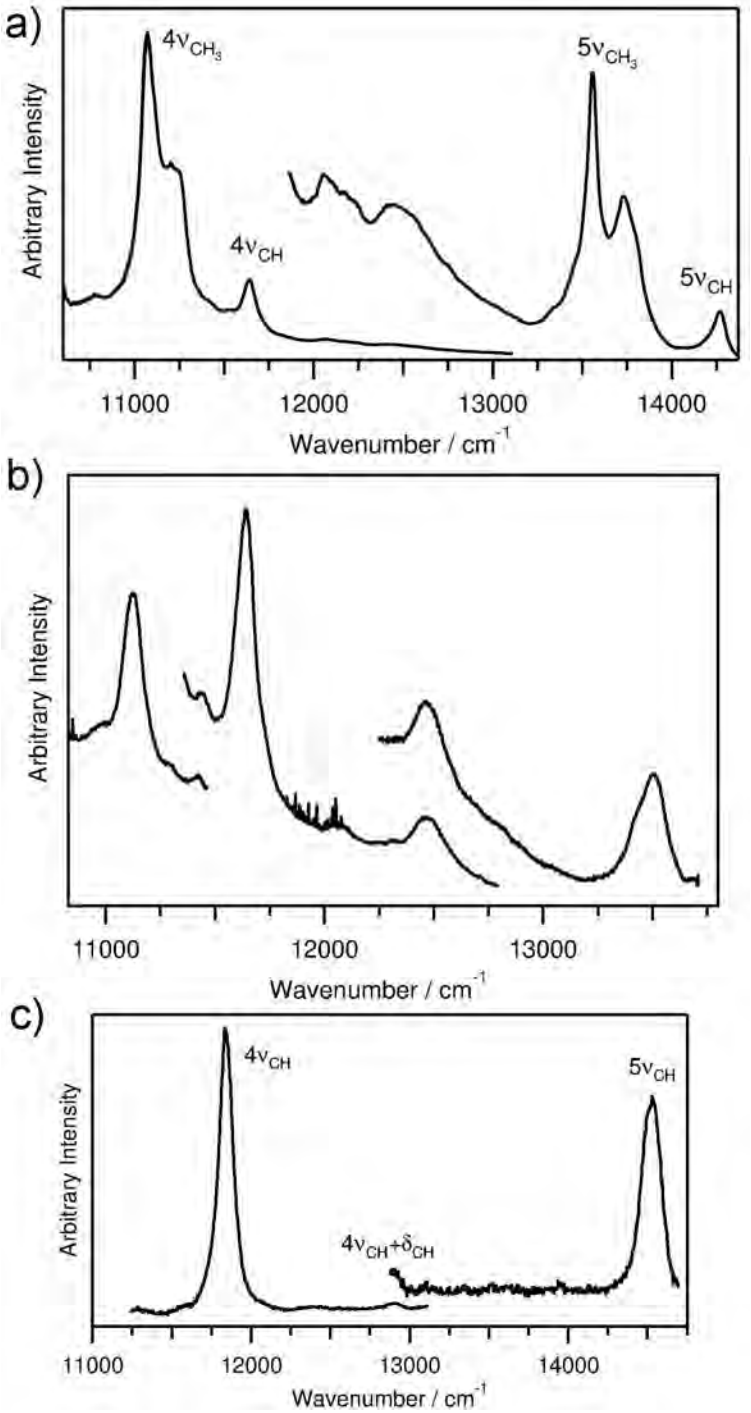

Figure 5: Room temperature photoacoustic spectra of a) 7 Torr AcAc vapor, b) 8 Torr AcAc-d_8 vapor, and c) 0.5 Torr hexafluoroacetylacetone vapor. The high frequency regions are expanded for more detail.

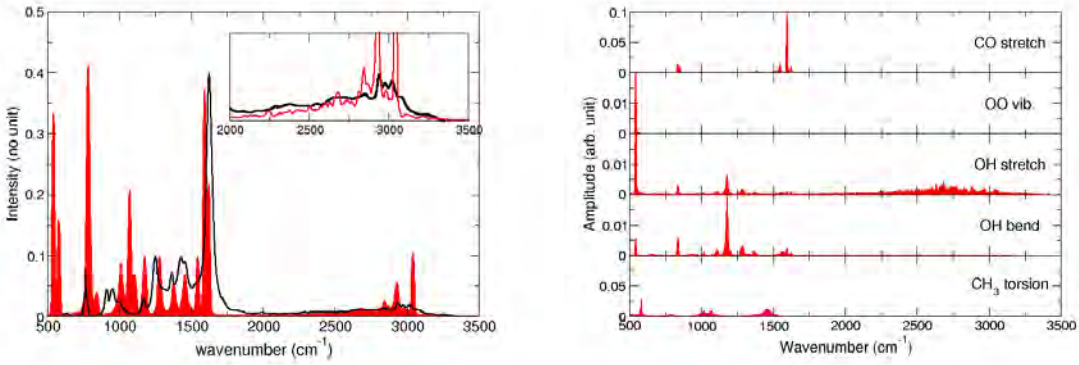

Figure 6: IR spectra computed from 5 ns NVE MD trajectories at 300 K: a) IR spectrum of AcAc in the gas phase, with the experimental spectrum superimposed; b) power spectra (from top to bottom) for CO stretch, OO stretch, OH stretch, OH bends, and the CH_3 torsion, respectively.

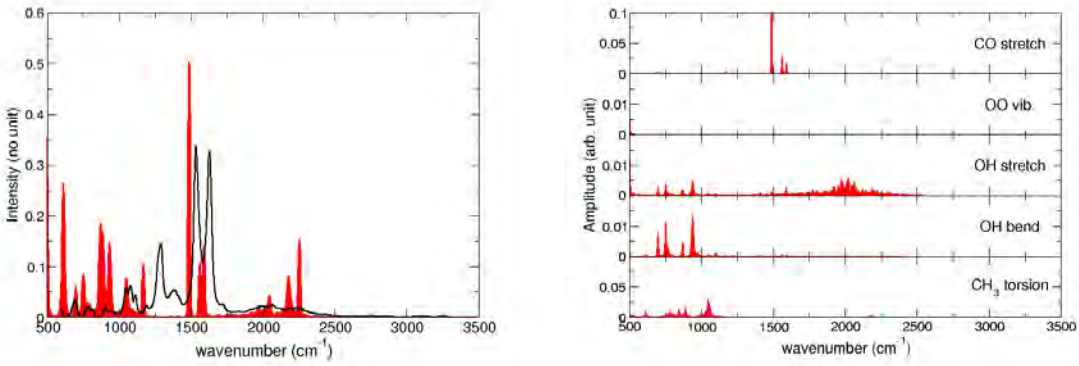

Figure 7: IR spectra computed from 5 ns NVE MD trajectories at 300 K: a) IR spectrum of AcAc-d_8 in the gas phase, with the experimental spectrum superimposed; b) power spectra (from top to bottom) for CO stretch, OO stretch, OH stretch, OH bends, and the CH_3 torsion, respectively.

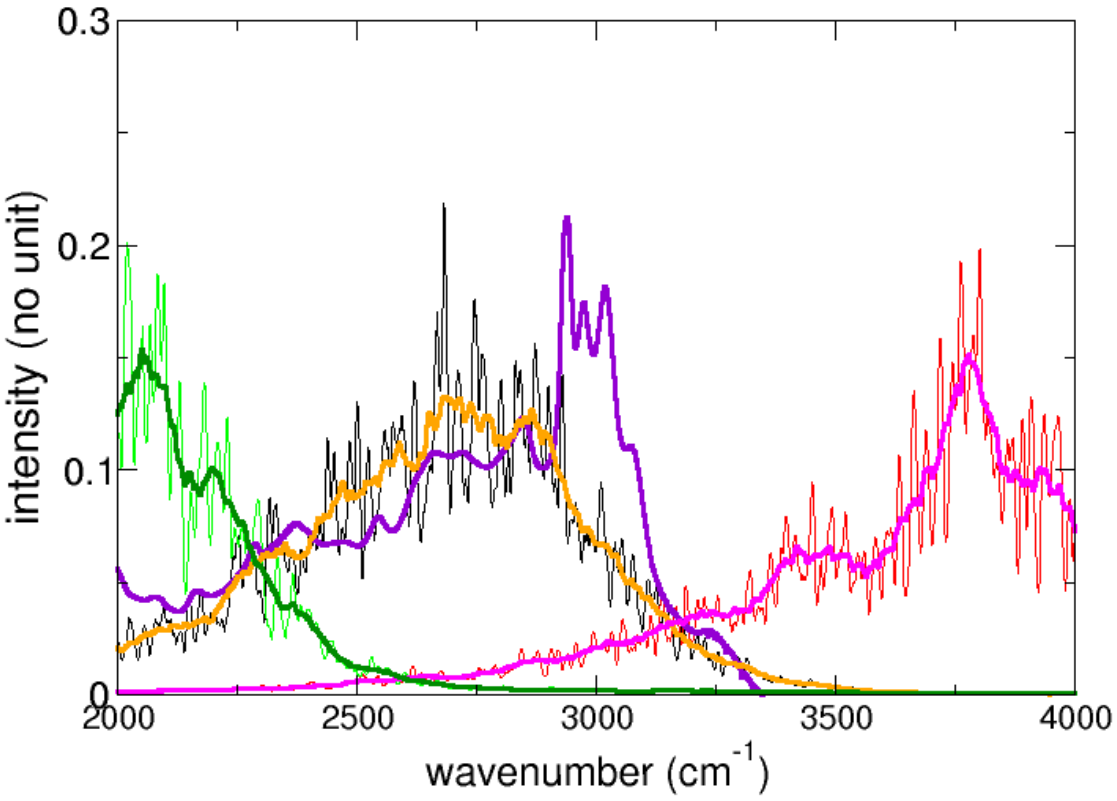

Figure 8: Effect of scaling the barrier for PT on the IR-band for AcAc. Comparison of the experimental spectrum (purple) in the PT-band region with those from simulations with different barrier heights of the MMPT PES: simulations with the reference PES - barrier height of 2.35 kcal/mol (orange, black), with half the barrier height (dark and light green) and with twice the barrier height (magenta and red). The pronounced peaks in the experimental spectrum around 3000 cm^{-1} correspond to CH stretch vibrations which do not appear in the computed power spectrum of the transferring hydrogen atom.